# Effects of mobility of small islands on growth in molecular-beam epitaxy

Itay Furman[*] and Ofer Biham[†]

*Racah Institute of Physics, The Hebrew University, Jerusalem 91904, Israel*

(Received 18 September 1996)

The effects of mobility of small islands on island growth in molecular-beam epitaxy are studied. It is shown that mobility of small islands affects both the scaling and morphology of islands during growth. Three microscopic models are considered, in which the critical island sizes are $i^* = 1$, 2, and 3 (such that islands of size $s \leq i^*$ are *mobile*, while islands of size $s \geq i^* + 1$ are *immobile*). As $i^*$ increases, islands become more compact, while the exponent $\gamma$, which relates the island density to deposition rate, increases. The morphological changes are quantified by using fractal analysis. It is shown that the fractal dimensions are rather insensitive to changes in $i^*$. However, the prefactors provide a quantitative measure of the changing morphologies. [S0163-1829(97)04012-5]

## I. INTRODUCTION

The growth of thin films in molecular-beam epitaxy involves atom diffusion on the surface and nucleation of islands, followed by aggregation and coalescence. The resulting morphology is found to depend on the detailed nature of microscopic diffusion processes on the substrate, as well as the deposition rate and substrate temperature. Scanning tunneling microscopy (STM) has revealed a variety of morphologies in the submonolayer regime. Compact islands of nearly square shape have been observed for homoepitaxial growth on fcc(001) substrates such as Ni(001) and Cu(001).[1,2] Fractal-like islands that resemble diffusion-limited aggregation[3] (DLA) clusters have been observed in systems such as Au on Ru(0001),[4] while Pt on Pt(111) was found to exhibit both fractal-like shapes and more compact, nearly triangular shapes.[5,6] Experimental studies and theoretical work using Monte Carlo simulations have shown that the submonolayer morphology depends on the rates of various diffusion processes on the substrate. In particular, systems that exhibit high atom mobility along island edges (typically on square substrates) tend to form compact islands. Low edge mobility gives rise to islands with DLA-like shapes (typically on hexagonal substrates). These morphologies are important beyond the submonolayer since they affect the multilayer growth mode of the film. The island morphology also affects the Schwoebel barrier[7] for an atom deposited on top of an island to hop down the step. When this barrier is large islands tend to nucleate on top of islands, resulting in three-dimensional growth mode, while a small barrier gives rise to layer-by-layer growth.

Scaling properties of island growth have been studied experimentally using statistical analysis of STM data and helium beam scattering.[8–14] Theoretical studies have applied rate equations[15–21] as well as Monte Carlo (MC) simulations.[22–35] It was found that for a broad class of systems a short transient regime is followed by a quasi-steady-state where a scaling relation of the form

$$N \sim \left( \frac{F}{4h} \right)^{\gamma} \tag{1}$$

applies, where $N$ is the island density, $F$ is the flux or deposition rate, and $h$ is the adatom diffusion coefficient (note that the hopping rate for an isolated adatom is $4h$ due to the four possible directions for hopping). The exponent $\gamma$ depends on microscopic properties such as the stability[32] and mobility[17,36] of small islands, isotropic vs anisotropic diffusion,[2,8,34] and the existence of magic islands (namely, islands that are stable, while larger islands are unstable).[31] It was found that for systems in which the smallest stable island is of size $i^* + 1$ (where islands of size $s \leq i^*$ dissociate), in the asymptotic limit of slow deposition rate, for isotropic diffusion, $\gamma = i^* / (i^* + 2)$. Experimentally, it was found that $\gamma$ may depend on temperature.[10,13] For example, for fcc(001) surfaces a transition from $i^* = 1$ to $i^* = 3$ due to temperature increase was characterized, where the transition temperature is determined by the ratio between the aggregation and dissociation rates of dimers and trimers.[37] The island size distribution was also studied and found to depend on $i^*$. These studies revealed that scaling properties can be used to identify microscopic processes at the atomic level and to estimate various activation energies that are difficult to measure. Experimental measurements of some diffusion processes at the atomic level are possible using field ion microscopy. This technique was used to identify diffusion modes for small islands such as dimers and trimers on fcc(001) metal surfaces and to measure their diffusion coefficients.[38]

In this paper we consider the relation between the scaling and morphology of the growing islands and trace them to properties of the microscopic model. In particular, we examine the effect of the *mobility* of small islands on island morphology and scaling. To this end we introduce a class of three microscopic models on a square substrate that differ in their diffusion properties. In model I only single atoms (monomers) are mobile [which means that the energy barrier for breaking a nearest-neighbor (NN) or a next-nearest-neighbor (NNN) bond is practically infinite]. In model II both monomers and dimers (clusters of two atoms) are mobile, while in model III monomers, dimers, and trimers (clusters of three atoms) are mobile. An island is defined as a cluster of adatoms connected by NN or NNN bonds. The island size $s$ is the number of atoms in the island. In this paper we do not consider island instability, but only island

mobility. Therefore, we define the critical island size $i*$ as the size for which all islands of size $s \leq i*$ are mobile, while islands of size $s \geq i*+1$ are immobile. Thus $i*=1, 2$, and 3 for models I, II, and III, respectively. Note that in the models considered here islands are stable even for $s \leq i*$ in the sense that there is no detachment of atoms from islands. However, due to their mobility these small islands tend to collide and merge into other islands.

The models we consider involve only local (NN and NNN) interactions such that the hopping rate for an atom in each of the four possible directions is determined by the occupancy in a neighborhood of $3 \times 3$ sites around it. We show that in this type of model there is a correlation between mobility of small islands and edge mobility. In model I, once an adatom attaches to an island edge as a NN it cannot move and therefore edge mobility is completely suppressed. Model II allows very limited edge mobility, while model III allows more moves, including hopping around a corner of an island. As the edge mobility increases islands become more compact because it tends to suppress narrow fingers and allows the atoms to find more stable positions with more nearest and next-nearest neighbors.

The correlation between mobility of small islands and edge mobility gives rise to a relation between the scaling properties determined by the critical island size and the morphology that depends on the edge mobility. To quantify this relation we first obtain the scaling exponent $\gamma$ for the three models using both rate equations and MC simulations. We then examine the island morphology for the three models and apply a fractal analysis using the box-counting algorithm and mass dimension evaluation.[39] The box-counting function, in the scaling regime, can be described by

$$N_B(l) = A_B l^{-D_B}, \qquad (2)$$

where $l$ is the box size, $N_B(l)$ is the number of boxes that contain at least one atom, $D_B$ is the box-counting fractal dimension, and $A_B$ is the prefactor. We find that the fractal dimension $D_B$ is rather insensitive to the differences between the models. The prefactor $A_B$, however, provides a quantitative measure of the different morphologies. Similar conclusions are obtained for the mass dimension $D_M$ and its prefactor $A_M$.

The paper is organized as follows. The models are introduced in Sec. II. Scaling properties of island growth and their dependence on the microscopic model are presented in Sec. III. The morphologies are examined in Sec. IV, followed by a discussion in Sec. V and a summary in Sec. VI.

## II. MODELS

To study the scaling and morphology during island growth we introduce three models of diffusion on the square lattice. Submonolayer thin-film growth during deposition in molecular-beam epitaxy is then studied using kinetic MC simulations.[40] In these simulations atoms are deposited randomly on the square substrate at a rate $F$ [given in monolayers (ML) per second] and hop according to the microscopic model. The hopping rate $h$ (in units of hops per second) for a given atom to each unoccupied NN site is given by
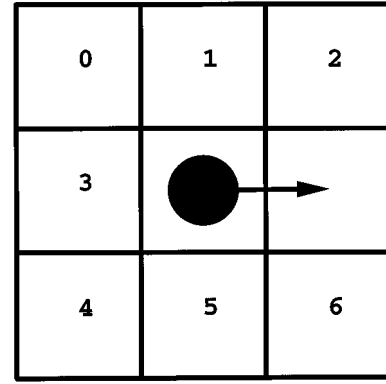
$$h = \nu \exp(-E_B/k_B T), \qquad (3)$$



FIG. 1. Local environment of a hopping atom. Each one of the seven adjacent sites $k = 0, \dots, 6$ can be either occupied ($S_k = 1$) or unoccupied ($S_k = 0$), giving rise to $2^7 = 128$ local environments with activation energies $E_B^n$, $n = 0, \dots, 127$, where $n = \Sigma_{k=0}^{6} S_k 2^k$.

where $\nu = 10^{12}$ s$^{-1}$ is the attempt frequency, $E_B$ is the energy barrier, $k_B$ is the Boltzmann factor, and $T$ is the temperature. The coverage after time $t$ is then $\theta = Ft$ (in ML).

In our MC simulations moves are selected randomly from the list of all possible moves at the given time with the appropriate weights. The time is then advanced according to the inverse of the sum of all rates. In the models used here the energy barrier $E_B$ for hopping is determined by the local environment in a $3 \times 3$ square around the hopping atom (Fig. 1), where the occupancy of seven adjacent sites, $k = 0, \dots, 6$, is taken into account. Each one of these sites can be either occupied ($S_k = 1$) or vacant ($S_k = 0$), giving rise to $2^7 = 128$ barriers. To index them we use the binary representation where the energy barriers are $E_B^n$, $n = 0, \dots, 127$ and $n = \Sigma_{k=0}^{6} S_k 2^k$. Using this indexing, we introduce three models of nearest-neighbor hopping on the surface (Fig. 2). In model I only monomers are mobile, in model II dimers are also mobile, and model III includes mobility of trimers as well. To simplify the analysis, our models include only one hopping rate, obtained by assigning the same activation energy ($E_B = 0.5$ eV) to all the allowed moves and a very high (practically infinite) energy barrier for all moves that are not allowed in the given model. The models are minimal in the sense that they include only the minimal set of moves required to achieve the specified island mobility. Some more moves can be added without modifying $i*$ (see Sec. V). Note that in our models there is no additional barrier for hopping down a step, which is justified for small islands and especially for fractal-like ones.[30] Atoms deposited on top of an island hop until they hit the edge and hop down to be incorporated into the island. Nucleation of a second layer is thus suppressed. The models are used to perform a systematic study of the effects of mobility of small islands on the scaling and morphology of the growing islands. The three models are introduced below.

### A. Model I

In this model only monomers can move [Fig. 2(a)]. Atoms cannot move away from NN or NNN atoms, while they can move towards a NNN atom, making it a NN (moves 4, 64, and 68 in Fig. 2). The latter moves are included to en-
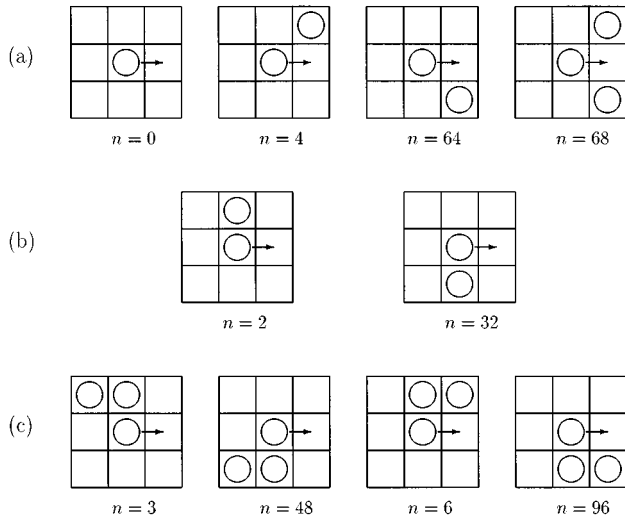
(a)



(b)

FIG. 2. Moves included in the three models. Model I includes only the moves in (a). Model II includes the moves in (a) and (b), while model III includes all the moves in (a), (b), and (c). All the allowed moves have the same activation energy $E_B$, while the activation energy for all other moves is practically infinite.
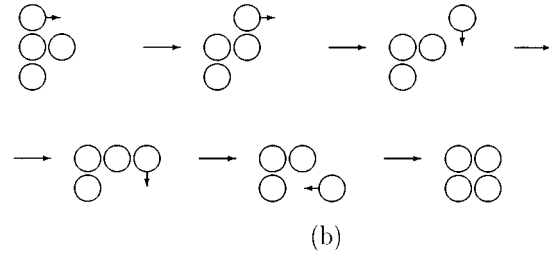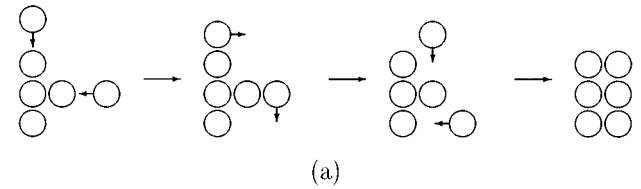
FIG. 3. Effect of allowing more moves on island morphology, making islands more compact. (a) The effect of allowing moves 2 and 32 on the structure of a six-atom island. (b) The effect of allowing moves 3, 48, 6, and 96 on the structure of a four-atom island.

hance adatom association and the creation of islands. (Note that in this model none of the allowed moves involve bond breaking.)

### B. Model II

Here both monomers and dimers are mobile. In addition to the moves included in model I two new moves are added [Fig. 2(b)]. Dimer mobility is now possible via a combination of a bond-breaking (move 2 or 32) and a bond-building move (move 4 or 64). These additional moves introduce more channels for island rearrangements, which lead to a more compact island shape [Fig. 3(a)].

### C. Model III

In this model trimers are mobile too. Four moves are added to those present in model II (moves 3, 6, 48, and 96), which are required for trimer mobility [Fig. 2(c)]. They also enhance the mobility of atoms on island edges and in particular allow for an edge adatom to move around a corner [Fig. 3(b)]. Note, however, that edge mobility in this model is still highly limited. For example, an atom adjacent to a straight long edge is immobile even in model III.

### D. Diffusion coefficients

To confirm that the critical island size is indeed $i^* = 1,2,3$ for models I, II, and III, respectively, and to obtain the diffusion coefficients of mobile islands in each model we have done simulations of single cluster diffusion. To obtain the statistics required for a precise determination of the diffusion coefficients we performed 1000 runs for monomers, dimers, trimers, and tetramers (islands of four atoms) in each of the three models. Each run was carried out to time equal to 0.6 s, which is about 200 times larger than the time scale for hopping at the given temperature ($T = 250$ K). The diffusion coefficients were obtained from the relation

$\langle r^2 \rangle = 4h_s t$, $s = 1,2,3,4$, where $r$ is the distance between the initial position of the center of mass of the cluster and its position after time $t$, $h_s$ is the diffusion coefficient for a cluster of size $s$, and $\langle \rangle$ represents an average over the 1000 runs. The diffusion coefficients for monomers, dimers, trimers, and tetramers in each of the three models are shown in Table I.[41] Our expectations are confirmed, namely, that in model I only monomers are mobile, in model II dimers are mobile as well, and in model III also trimers are mobile.

### III. SCALING PROPERTIES

The submonolayer growth is typically divided into three stages: the early stage is dominated by island nucleation followed by an aggregation-dominated stage until coalescence sets in. In the aggregation stage the density of stable islands $N$ exhibits power-law behavior as a function of the ratio between the deposition rate and the adatom hopping rate of the form $N \sim (F/4h)^\gamma$. The exponent $\gamma$ is determined by the microscopic processes that are activated on the surface during growth. In the case where all clusters of size $s \leq i^*$ are mobile, while larger clusters are immobile, the asymptotic

TABLE I. Diffusion coefficients of small islands as measured from MC simulations of single islands for the three presented models at $T = 250$ K. It is shown that $i^* = 1$, 2, and 3 for models I, II, and III, respectively.

| Cluster size | Diffusion coefficients (hops/s) | | |
| --- | --- | --- | --- |
| | Model I | Model II | Model III |
| 1 | $82 \pm 2$ | $82 \pm 2$ | $84 \pm 2$ |
| 2 | 0.0 | $21 \pm 1$ | $21 \pm 1$ |
| 3 | 0.0 | 0.0 | $7.7 \pm 0.5$ |
| 4 | 0.0 | 0.0 | 0.0 |

value of $\gamma$ in the limit where $F/h \to 0$ is given by[17]

$$\gamma = \frac{i^*}{2i^*+1}. \qquad (4)$$

This result is exact if all mobile islands have the same diffusion coefficient, namely, $h_s = h$, $s = 1, \ldots, i^*$. Still, it is a good approximation if all the diffusion coefficients are of the same order of magnitude and the ratios between them are independent of the temperature, as is the case for the models studied in this paper.

To study the scaling properties of island growth with mobility of small islands, for experimentally relevant deposition rates, we introduce a set of rate equations that describe the time evolution of the densities of mobile and immobile islands. In these equations, islands including $s$ atoms are mobile for $1 \leq s \leq i^*$ with diffusion coefficient $h_s$ and immobile for $s \geq i^* + 1$. The density of mobile islands of size $s$ is given by $x_s$, $1 \leq s \leq i^*$, while the total density of immobile islands is given by $N$. Both densities are normalized per lattice site and the lattice constant is taken to be 1. The rate equations take the form

$$\dot{x}_1 = F - \sum_{i=1}^{i^*} 4(h_1 + h_i)x_1 x_i - 4h_1 x_1 N, \qquad (5a)$$

$$\dot{x}_s = \sum_{i=1}^{i^*} 2(h_i + h_{s-i})x_i x_{s-i} - \sum_{i=1}^{i^*} 4(h_i + h_s)x_i x_s - 4h_s x_s N,$$

$$2 \leq s \leq i^* \quad (5b)$$

$$\dot{N} = \sum_{i=1}^{i^*} \sum_{j=i^*+1-i}^{i^*} 2(h_i + h_j)x_i x_j, \qquad (5c)$$

where the density of immobile islands $N$ is given by

$$N \equiv \sum_{s=i^*+1}^{\infty} x_s. \qquad (6)$$

The first term in Eq. (5a) describes the deposition of new atoms, while the first term in Eq. (5b) describes the building of mobile islands by merging of two mobile islands of smaller sizes. The second and third terms in Eqs. (5a) and (5b) describe the reduction in the number of mobile islands of size $s$ due to their collision with other mobile and immobile islands, respectively. Equation (5c) describes the rate of nucleation of immobile islands due to collision of two mobile islands.

A rate equation representation of models I, II, and III can be obtained from Eqs. (5) when $i^* = 1$, 2, and 3, respectively, and with the diffusion coefficients $h_i$ given in Table I. Note that the rate equations provide a mean-field description ignoring spatial correlations. Moreover, since we concentrate here on the effects of mobility of small islands, other processes such as atom detachment from islands, atoms deposited on top of islands, and coalescence are not included in the equations. Also, for simplicity, the capture number is taken as a constant. In general, it is found to depend on both the island size and the coverage.[27]

TABLE II. Comparison of $\gamma$ obtained from asymptotic analysis and numerical integration of rate equations and from MC simulations, for models I, II, and III. The numerical results for both the rate equations and MC simulations were obtained at the same coverage $\theta = 0.2$ and for the same range of deposition rate $F = 10^{-6} - 10^{-2}$ ML/s at $T = 250$ K.

| Model | Rate equations | | Simulation |
| | Asymptotic | Numerical | |
| --- | --- | --- | --- |
| I | $1/3 = 0.333$ | $0.31 \pm 0.01$ | $0.36 \pm 0.01$ |
| II | $2/5 = 0.400$ | $0.36 \pm 0.01$ | $0.38 \pm 0.01$ |
| III | $3/7 = 0.430$ | $0.37 \pm 0.01$ | $0.41 \pm 0.01$ |

We have examined Eqs. (5) in the aggregation regime using asymptotic analysis of the type described in Ref. 19. In this analysis Eqs. (5) are written in dimensionless form using $\hat{x}_s = l_1^2 x_s$, $\hat{N} = l_1^2 N$, and $\hat{t} = t/t_1$, where $l_1 = (4h/F)^{1/4}$ and $t_1 = (4hF)^{-1/2}$. We then consider the aggregation stage $(\hat{t} \gg 1)$ assuming that $\hat{N} \gg \hat{x}_1 \gg \cdots \gg \hat{x}_i^*$ Since at this stage the density of mobile islands is approximately constant we solve Eqs. (5) in its dimensionless form for $\dot{\hat{x}}_s = 0$, $1 \leq s \leq i^*$. This is done using the ansatz that $\hat{x}_s \sim \hat{t}^{\alpha s + \beta}$ and $\hat{N} \sim \hat{t}^{\delta}$, where $\alpha$, $\beta$, and $\delta$ are constants to be determined from the solution. Solving for the leading order in each equation, we find scaling relations for the densities of immobile and mobile islands as a function of $F/4h$ and $\theta$:[42]

$$x_s \sim (F/4h)^{(i^*+s)/(2i^*+1)} \theta^{-(2s-1)/(2i^*+1)}, \quad s = 1, 2, \ldots, i^* \qquad (7a)$$

$$N \sim (F/4h)^{i^*/(2i^*+1)} \theta^{1/(2i^*+1)}. \qquad (7b)$$

For models I, II, and III we find $\gamma = 1/3$, $2/5$, and $3/7$, respectively. It is important to note that these results are only asymptotically exact in the limit $F/4h \to 0$. Numerical integration of the rate equations shows slow convergence to these results as the deposition rate is lowered. In Table II we present the values for $\gamma$ obtained from numerical integration of Eq. (5) with diffusion coefficients $h_i$, taken from Table I, together with the asymptotic values.

To complement these results we have also examined the scaling of island density $N$ vs deposition rate $F$, using MC simulations (Fig. 4). The island density obtained in these simulations for the three models, as a function of deposition rate, is shown in Fig. 4 for coverage of $\theta = 0.2$ and substrate temperature $T = 250$ K. Each data point in this figure represents an average over 100 runs and the lattice size is $250 \times 250$ in all the runs. The values of $\gamma$ for the three models, obtained from the MC results in Fig. 4, are summarized in Table II. It is observed that $\gamma$ increases as $i^*$ is increased and this trend appears in all three columns of Table II representing the asymptotic result, rate equations, and MC simulations. This can be intuitively understood from the following qualitative argument. In the limit of very fast deposition rate (say, $F/4h \cong 1$) the effect of island mobility is negligible and the island density is very large and nearly independent of $i^*$. As $F/4h$ is decreased the mobility of single atoms and islands of size $s \leq i^*$ gives rise to nucleation of fewer and larger islands. This process is enhanced as
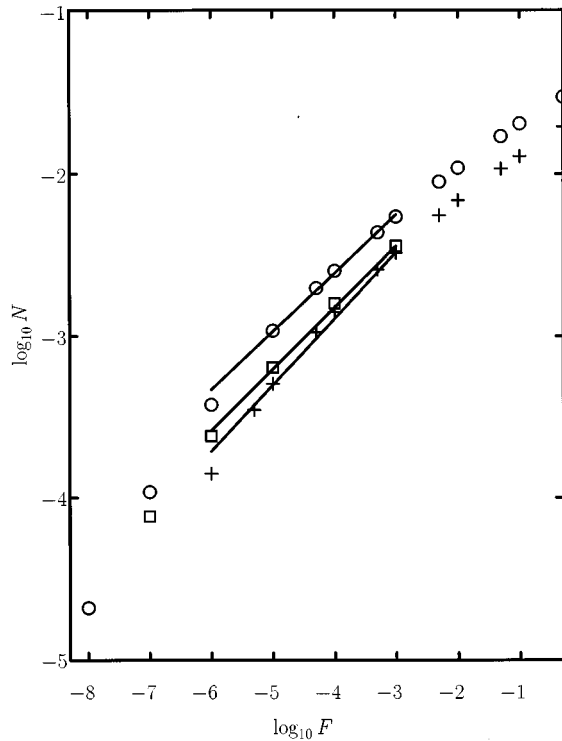
FIG. 4. Island density $N$ (islands/site) plotted vs deposition rate $F$ ML/s on a log-log scale for MC simulations of models I ($\bigcirc$), II ($\square$), and III ($+$) (with $i^* = 1$, 2, and 3, respectively) at coverage of $\theta = 0.2$ and substrate temperature $T = 250$ K. The exponent $\gamma$, given by the slope, increases as $i^*$ is increased. The results for $\gamma$ are summarized in Table II.

$i^*$ increases since it adds more channels for collision and merging of islands. This results in a faster decrease of $N$ as a function of $F/4h$.

The values of $\gamma$ for rate-equation integration at a finite rate are found to be lower than the asymptotic value. The $\gamma$ values for MC simulations are higher than the corresponding rate-equation values, which can be attributed to spatial correlations and coalescence, which are not taken into account in the rate equations. Wolf[31] proposed an alternative formula for the exponent $\gamma$, which takes into account the fractal dimension of the islands denoted by $D_f$. Adapted to our case, it takes the form

$$\gamma = \frac{2i^*}{4i^* + D_f},  \quad (8)$$

which coincides with Eq. (4) for compact islands ($D_f = 2$). Note that Eq. (8) implies that $\gamma$ for fractal islands is larger than for compact islands with the same $i^*$, giving rise to lower densities of islands.[31] This is reasonable since fractal islands have a larger effective area per given mass. Thus they inhibit more efficiently new nucleation events, which results in a smaller island density, $N$. Since the numerical simulations generate fractal-like islands while the rate equations assume pointlike (and thus compact) islands this might provide a further explanation for the tendency of the MC exponents to be larger than the exponents obtained from numerical integration of the rate equations.
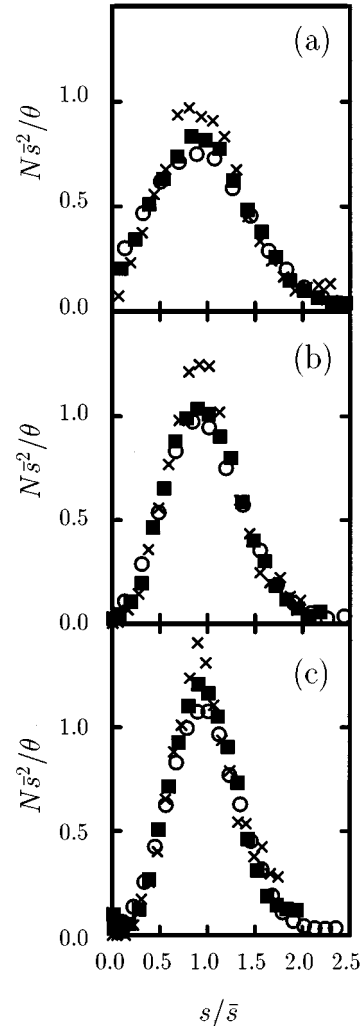


FIG. 5. Scaled island size distribution vs scaled size for (a) model I, (b) model II, and (c) model III. The deposition rates are $F = 10^{-3}$ ML/s ($\bigcirc$), $F = 10^{-4}$ ML/s ($\blacksquare$), and $F = 10^{-5}$ ML/s ($\times$) and the coverage is $\theta = 0.2$. Note that the peak narrows as $i^*$ increases.

The scaling properties of the island size distribution have been studied both experimentally[12] and theoretically.[18,24,31,32] These studies indicated that the island size distribution strongly depends on the stability and mobility of small islands and is modified in the case of magic islands.[31] The scaled island size distributions for models I, II, and III are presented in Figs. 5(a)–5(c). Here $\bar{s}$ is the average island size. For all three models the deposition rates are $F = 10^{-3}$ $10^{-4}$, and $10^{-5}$ ML/s. We observe that as $i^*$ increases the peaks rise more slowly on the left-hand side (small $s/\bar{s}$) due to the depletion of the mobile islands. They also fall off more sharply on the right-hand side and thus become narrower. This trend is qualitatively similar to previous results for the case where small islands are unstable. Note that the peak height increases considerably as $F$ decreases. This may be due to coalescence, which is found to become more pronounced as the deposition rate decreases. Coalescence causes $\bar{s}$ to increase, pushing up the scaled island size distribution, which includes the factor $\bar{s}^2/\theta$.
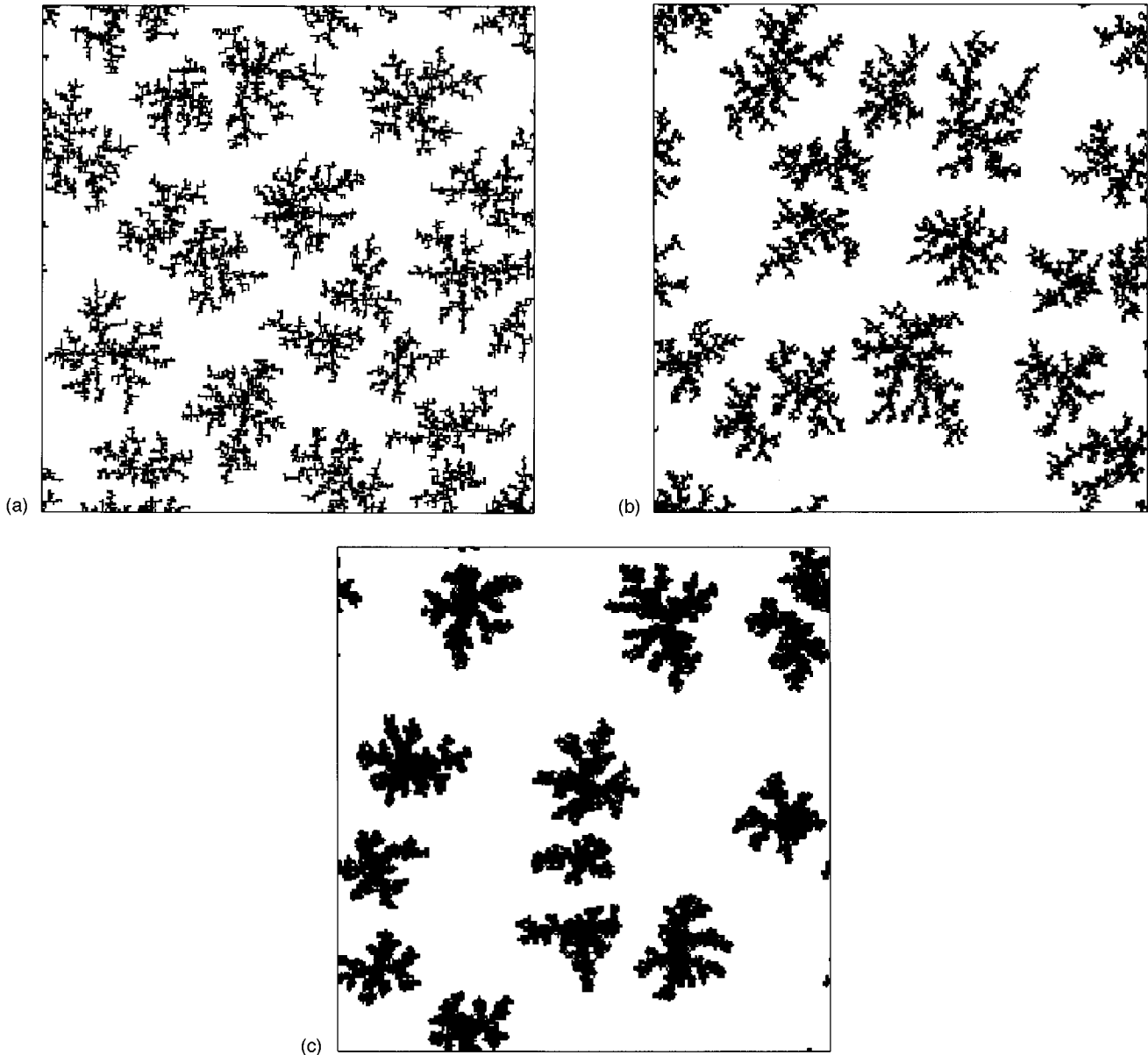
FIG. 6. Top view of the surface layer under growth conditions specified by models I (a), II (b), and III (c) for deposition rate of $F = 10^{-6}$ ML/s, coverage $\theta = 0.2$, and substrate temperature $T = 250$ K. The deposited atoms and islands are represented by the dark color and the exposed substrate is white. Lattice size: $250 \times 250$ sites.

## IV. MORPHOLOGY

To examine the relation between mobility of small islands and island morphology we have performed extensive MC simulations of island growth using the three models described above. The morphology of the growing islands is shown in Fig. 6 for deposition rate $F = 10^{-6}$, coverage $\theta = 0.2$, and $T = 250$ K. The morphology obtained for model I [Fig. 6(a)] best resembles the shape of small DLA clusters grown on the square lattice, due to the suppressed edge mobility. The islands of models II and III [Figs. 6(b) and 6(c), respectively] exhibit wider arms and have more compact shapes due to edge mobility associated with the increased $i^*$. To quantify these observations we have performed fractal analysis of the island morphology using the box-counting algorithm and mass dimension evaluation for the three models. In the box-counting technique one divides the lattice into boxes of linear size $l$ and counts the number of boxes $\langle N_B(l) \rangle$ (averaged over a series or runs) that intersect the set of islands. The box-counting dimension $D_B$ is then given by

$$\log_{10}\langle N_B(l) \rangle = \log_{10}A_B - D_B\log_{10}l, \qquad (9)$$

where $A_B$ is a prefactor. The box-counting function $N_B(l)$ for the three models is shown in Fig. 7 on a log-log scale. The fractal dimensions are presented in Table III and the prefactors in Table IV. It is shown that although the three models generate different looking morphologies, the box-counting dimension $D_B$ for a given deposition rate and coverage is practically independent of the model. The box-counting dimensions are found to be typically lower than the DLA dimension $D_{\text{DLA}} \cong 1.72$ and increase as the deposition rate decreases. A significant difference between the models is reflected in the coefficient $A_B$. It is shown (Table IV) that
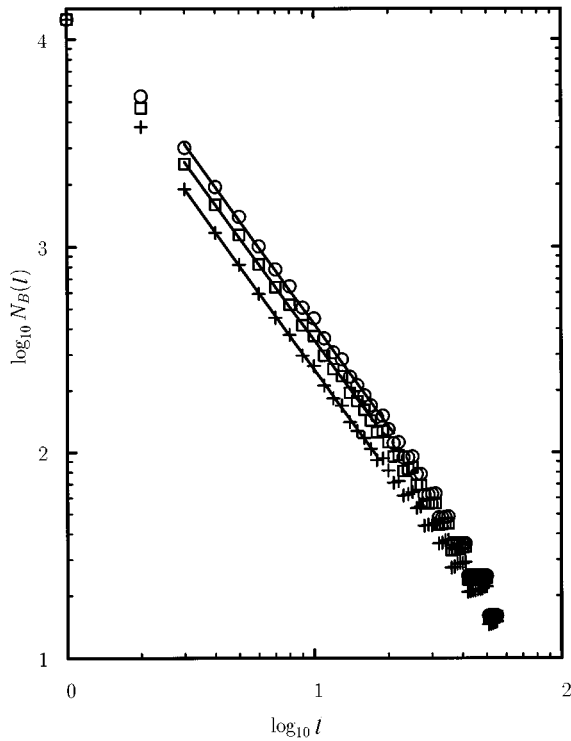
FIG. 7. Box counting function that counts the number $N_B(l)$ of occupied boxes vs box size $l$ shown for the island morphology obtained from models I ($\bigcirc$), II ($\square$), and III ($+$) at deposition rate $F=10^{-7}$ ML/s, coverage $\theta=0.2$, and substrate temperature $T=250$ K. Note that the slopes are found to be the same for the three models, indicating that the fractal dimension $D_B$ in insensitive to the small island mobility (Table III). However, the intercept (determined by the prefactor $A_B$) is different for the three models (Table IV).

as $i^*$ increases and islands become more compact, $A_B$ decreases by almost a factor of 2. It also decreases when deposition rate is increased (which also results in more compact islands). The behavior of $A_B$ can be understood from the fact that as islands become more compact each occupied box tends to include more atoms (and still it is counted only once). Since the coverage is maintained the number of occupied boxes must decrease.

Unlike the box-counting analysis, which is done on the entire system, the mass dimension analysis is done on each island separately. In this analysis one finds the center of mass of the island and measures the total mass of the atoms $M(r)$ bounded by a circle of radius $r$ around it as a function of $r$. The mass dimension $D_M$ is then obtained from (Fig. 8)

$$\log_{10}\langle M(r)\rangle = \log_{10}A_M + D_M\log_{10}r, \qquad (10)$$

TABLE III. Box-counting dimension $D_B$, for models I, II, and III at three deposition rates $F$, coverage $\theta=0.2$, and $T=250$ K. The dimensions are typically lower than the DLA dimension and are only weakly dependent on the model.

| Model | $F=10^{-6}$ (ML/s) | $F=10^{-7}$ (ML/s) | $F=10^{-8}$ (ML/s) |
|---|---|---|---|
| I | $1.62\pm0.01$ | $1.66\pm0.01$ | $1.68\pm0.02$ |
| II | $1.59\pm0.01$ | $1.64\pm0.01$ | $1.66\pm0.02$ |
| III | $1.59\pm0.01$ | $1.67\pm0.01$ | $1.72\pm0.02$ |

TABLE IV. Prefactor $A_B$ in Eq. (9) for the three models for various deposition rates $F$, coverage $\theta=0.2$, and $T=250$ K. Entries are in units of $10^3$ boxes. The prefactor is strongly dependent on the model reflecting the morphological changes.

| Model | $F=10^{-6}$ (ML/s) | $F=10^{-7}$ (ML/s) | $F=10^{-8}$ (ML/s) |
|---|---|---|---|
| I | $18.7\pm0.5$ | $19.4\pm0.5$ | $20.2\pm0.5$ |
| II | $14.7\pm0.5$ | $15.6\pm0.5$ | $15.90\pm0.5$ |
| III | $10.9\pm0.5$ | $11.9\pm0.5$ | $12.0\pm0.5$ |

where the average is over a large number of islands. The values of the mass dimension $D_M$ obtained for the three models are summarized in Table V and the prefactors $A_M$ in Table VI. The mass dimension is found to be in the range between 1.83 and 1.91, significantly larger than the DLA dimension. This larger dimension reflects the enhanced compactness of the islands; however, its dependence on the model is rather weak. The morphological differences are strongly reflected in the coefficient $A_M$, which increases as $i^*$ is increased. This trend of $A_M$ results from the fact that as the islands become more compact the mass included in a circle of radius $r$ around their center must increase. We conclude that the scaling properties reflected in $D_B$ and $D_M$ are weakly dependent on the models, while the prefactors $A_B$ and $A_M$ are strongly model dependent. In all the three models we considered, edge mobility is limited and allows only
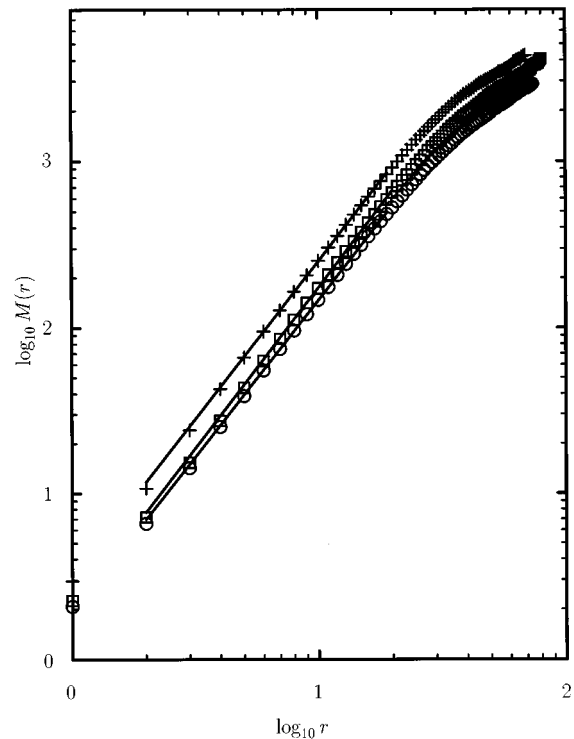


FIG. 8. Mass $M(r)$ within a circle of radius $r$ around the center of mass of an island vs $r$ for islands obtained from models I ($\bigcirc$), II ($\square$), and III ($+$) at deposition rate $F=10^{-7}$ ML/s, coverage $\theta=0.2$, and substrate temperature $T=250$ K. The mass dimension is given by the slope on the log-log scale. It is shown that the mass dimension $D_M$ is insensitive to the different morphologies obtained from these models (Table V). However, the prefactor $A_M$ shows significant differences (Table VI).

TABLE V. Mass dimension $D_M$, for models I, II, and III at various deposition rates $F$, coverage $\theta=0.2$, and $T=250$ K. The dimensions are considerably higher than the DLA dimension, but only weakly dependent on the model.

| Model | $F=10^{-6}$ (ML/s) | $F=10^{-7}$ (ML/s) | $F=10^{-8}$ (ML/s) |
|-------|--------------------|--------------------|--------------------|
| I     | $1.84\pm0.02$      | $1.89\pm0.02$      | $1.83\pm0.02$      |
| II    | $1.89\pm0.02$      | $1.94\pm0.02$      | $1.83\pm0.02$      |
| III   | $1.91\pm0.02$      | $1.90\pm0.02$      | $1.88\pm0.02$      |

local rearrangements of the structure. The prefactors (which are related to the curve intercept, i.e., to small scales) are sensitive to such changes. In contrast, the fractal dimensions that are determined over a range of scales are rather insensitive to the small-scale behavior.

Note that in model I the diffusion is similar to the DLA model. However, unlike DLA, atoms are added at a finite rate, nucleating a finite density of islands. Also, these atoms are deposited randomly from above rather than from boundaries located far away from the cluster as in DLA. Therefore, some of the atoms fall between (or on top of) the arms of the island. For these atoms the aggregation process is not diffusion limited. The DLA limit can be approached only when both $F/4h\rightarrow0$ and $\theta\rightarrow0$. The first limit is required in order to keep islands far away from each other. The second limit is required in order to ensure that the islands are very small compared to the area from which they draw atoms.

## V. DISCUSSION

The fractal analysis can provide useful information about processes and rates in island growth systems. It is accessible experimentally and can be done using either STM data[4] or helium beam scattering.[43] In the latter case, one possibility is to obtain the fractal dimension of contours of constant electron density of the monolayer from measurements of the specular peak intensity as a function of helium incidence energy.

Note that the models studied here, in particular models II and III, are minimal in the sense that they include the minimal number of allowed moves for the given $i^*$. One can add some more moves to each of these models without changing $i^*$. For example, moves $n=$ 6 (96), 36 (66), and 70 (100) can be added to model II. These moves are obtained by taking the moves shown in Fig. 2(b) and placing atoms at site $k=2$ or $k=6$ or both (see Fig. 1). The moves appear in pairs due to the horizontal mirror symmetry such that the move in parentheses is the mirror image of the one that precedes it. Similarly, moves $n=$ 7 (112), 52 (67), 70 (100), and 71

TABLE VI. Prefactor $A_M$ in Eq. (9) for the three models for various deposition rates $F$, coverage $\theta=0.2$, and $T=250$ K. The prefactor is strongly dependent on the model and sensitive to the different morphologies.

| Model | $F=10^{-6}$ (ML/s) | $F=10^{-7}$ (ML/s) | $F=10^{-8}$ (ML/s) |
|-------|--------------------|--------------------|--------------------|
| I     | $2.1\pm0.1$        | $1.9\pm0.1$        | $2.3\pm0.1$        |
| II    | $2.5\pm0.1$        | $2.0\pm0.1$        | $2.9\pm0.1$        |
| III   | $3.3\pm0.1$        | $3.1\pm0.1$        | $3.5\pm0.1$        |

(116) can be added to model III. These additional moves have no significant effect on the scaling properties (since $i^*$ remains unchanged), but they enhance edge mobility, making the islands more compact. In particular, move 7 (112) allows atom mobility along straight island edges, which is not possible otherwise. However, we find that highly compact islands of nearly square shape observed on fcc(001) metal substrates such as Cu(001) and Ni(001) cannot be obtained with models that include only one hopping rate such as the models studied here. Such highly compact islands are obtained only when the hopping rate for moves along island edges such as 7 (112) are much larger than other hopping rates in the system, including the hopping rate of the monomer.[26,32,35] In contrast, systems in which atoms can detach from island edges and reattach elsewhere exhibit rather compact island shapes even when the detachment rate is considerably smaller than the hopping rate of the monomer.[28,44]

In the models studied here diffusion occurs via the motion of one atom at a time. Other diffusion mechanisms that involve concerted motion of two atoms have also been observed. In particular, the exchange move in which a substrate atom is displaced by an adatom and pops out into a NNN site of the original adatom position. On surfaces such as Al(001) (Ref. 45) and Pt(001) (Ref. 46) it was found that the energy barrier for exchange is lower than for hopping, indicating that this is the dominant diffusion mechanism on these surfaces. In a different type of concerted move, two atoms move together along the edge of an island. When the barrier for such a move is lower than moves involving single atoms in the island they may drive island diffusion.[47] Recent STM experiments indicate that for Ag(001) even large islands may diffuse as a result of the high edge mobility in these systems.[48]

Models related to those studied in this paper appear in the cluster-cluster aggregation problem, where DLA-like clusters aggregate at a finite density.[49,50] Jensen *et al.*[51] have recently studied a model of island growth in which edge mobility is suppressed while islands of all sizes can move rigidly (and thus $i^*=\infty$) while their diffusion coefficients decay according to $h_s\sim1/s^p$. In this model the simple relation between edge mobility and island mobility, which exists in the models of local interactions studied here, is broken. Due to the lack of edge mobility islands maintain their DLA-like shape, while the exponent $\gamma$, which depends on $p$, is varied.

## VI. SUMMARY

In summary, we have performed a systematic study of the effect of mobility of small islands on the scaling and morphology in island growth on surfaces. The exponent $\gamma$, which describes the dependence of island density on deposition rate, was examined, for experimentally relevant deposition rates, using both numerical integration of the rate equations and MC simulations. It was found that $\gamma$ increases as the critical island size $i^*$ is increased. This reflects the decrease in island density, which results from the possibility of small islands to move and merge. The asymptotic value of $\gamma$ in the limit of slow deposition rate is given by $\gamma=i^*/(2i^*+1)$. However, convergence to this asymptotic value by decreasing the deposition rate turns out to be slow for MC simulations and even for rate equations. In addition, $\gamma$ exhibits a

rather slow dependence on $i^*$ as it increases and is limited to the range $1/3 \leq \gamma \leq 1/2$. This indicates that using this scaling law to extract microscopic information on mobility of small islands from experimental results is hard and requires very precise measurement of $\gamma$.

The island morphology was found to become more compact as $i^*$ is increased. This reflects a general relation between edge mobility and small island mobility in models of short-range interactions. To quantify the morphological changes we have performed a fractal analysis of the island morphology using the box counting and mass dimensions. In both cases it was found that the fractal dimension is rather insensitive to changes in $i^*$; however, the morphological change is reflected in the value of the prefactors.

*Electronic address: itayf@ariel.fiz.huji.ac.il

†Electronic address: biham@cc.huji.ac.il

[1] E. Kopatzki, S. Gunther, W. Nichtl-Pecher, and R. J. Behm, Surf. Sci. **284**, 154 (1993).

[2] S. Gunther, E. Kopatzki, M.C. Bartelt, J. W. Evans, and R. J. Behm, Phys. Rev. Lett. **73**, 553 (1994).

[3] T. A. Witten and L. M. Sander, Phys. Rev. Lett. **47**, 1400 (1981).

[4] R. Q. Hwang, J. Schröder, C. Günter, and R. J. Behm, Phys. Rev. Lett. **67**, 3279 (1991).

[5] T. Michely, M. Hohage, M. Bott, and G. Comsa, Phys. Rev. Lett. **70**, 3943 (1993).

[6] M. Bott, T. Michely, and G. Comsa, Surf. Sci. **272**, 161 (1992).

[7] R. L. Schwoebel, J. Appl. Phys. **40**, 614 (1969); G. Ehrlich and F. Hudda, J. Chem. Phys. **44**, 1039 (1966).

[8] Y. W. Mo, J. Kleiner, M. B. Webb, and M. G. Lagally, Phys. Rev. Lett. **66**, 1998 (1991).

[9] J.-K. Zuo and J. F. Wendelken, Phys. Rev. Lett. **66**, 2227 (1991).

[10] H.-J. Ernst, F. Fabre, and J. Lapujoulade, Phys. Rev. B **46**, 1929 (1992); Phys. Rev. Lett. **69**, 458 (1992); Surf. Sci. Lett. **275**, L682 (1992).

[11] W. Li, G. Vidali, and O. Biham, Phys. Rev. B **48**, 8336 (1993); G. Vidali, O. Biham, H. Zeng, J.-S. Lin, and W. Li, in *The Structure of Surfaces IV*, edited by S. Y. Tong and X. Xide (World Scientific, Singapore, 1995).

[12] J. A. Stroscio and D. T. Pierce, Phys. Rev. B **49**, 8522 (1994).

[13] J.-K. Zuo, J. F. Wendelken, H. Durr, and C.-L. Liu, Phys. Rev. Lett. **72**, 3064 (1994).

[14] H. Durr, J. F. Wendelken, and J.-K. Zuo, Surf. Sci. Lett. **328**, L527 (1995).

[15] S. Stoyanov and D. Kashchiev, Current Topics Mater. Sci. **7**, 70 (1981).

[16] J. A. Venables, G. D. T. Spiller, and M. Hanbucken, Rep. Prog. Phys. **47**, 399 (1984).

[17] J. Villain, A. Pimpinelli, and D. Wolf, Comments Condens. Matter Phys. **16**, 1 (1992); J. Villain, A. Pimpinelli, L. Tang, and D. Wolf, J. Phys. (France) I **2**, 2107 (1992).

[18] M. C. Bartelt and J. W. Evans, Phys. Rev. B **46**, 12 675 (1992); M. C. Bartelt, M. C. Tringides, and J. W. Evans, *ibid.* **47**, 13 891 (1993).

[19] L. Tang, J. Phys. (France) I **3**, 935 (1993).

[20] A. Zangwill, in *Evolution of Surfce and Thin Film Microstructure*, edited by H. A. Atwater, E. Chason, M. Grabow, and M. Lagally, MRS Symposium Proceedings No. 280 (Materials Research Society, Pittsburgh, 1993).

[21] O. Biham, G. T. Barkema, and M. Breeman, Surf. Sci. **324**, 47 (1995).

[22] A. F. Voter, Phys. Rev. B **34**, 6819 (1986).

[23] S. Clarke and D. D. Vvedensky, J. Appl. Phys. **63**, 2272 (1988).

[24] M. C. Bartelt and J. W. Evans, Surf. Sci **298**, 421 (1993); J. W. Evans and M. C. Bartelt, J. Vac. Sci. Technol. A **12**, 1800 (1994).

[25] P. Smilauer, M. R. Wilby, and D. D. Vvedensky, Phys. Rev. B **48**, 4968 (1993).

[26] G. T. Barkema, O. Biham, M. Breeman, D. O. Boerma, and G. Vidali, Surf. Sci. Lett. **306**, L569 (1994).

[27] G. S. Bales and D. C. Chrzan, Phys. Rev. B **50**, 6057 (1994).

[28] C. Ratsch, A. Zangwill, P. Smilauer, and D. D. Vvedensky, Phys. Rev. Lett. **72**, 3194 (1994); C. Ratsch, P. Smilauer, A. Zangwill, and D. D. Vvedensky, Surf. Sci. **329**, L599 (1995).

[29] Z. Zhang, X. Chen, and M. G. Lagally, Phys. Rev. Lett. **73**, 1829 (1994).

[30] J. Jacobsen, K. W. Jacobsen, P. Stoltze, and J. K. Norskov, Phys. Rev. Lett. **74**, 2295 (1995).

[31] M. Schroeder and D. E. Wolf, Phys. Rev. Lett. **74**, 2062 (1995); D. E. Wolf, in *Scale Invariance, Interfaces, and Non-Equilibrium Dynamics*, Vol. 344 of *NATO Advanced Study Institute, Series B: Physics*, edited by M. Droz, A. J. McKane, J. Vannimenus and D. E. Wolf (Plenum, New York, 1994).

[32] J. G. Amar and F. Family, Phys. Rev. Lett. **74**, 2066 (1995); Thin Solid Films **272**, 208 (1996); F. Family and J.G. Amar, Mater. Sci. Eng. B **30**, 149 (1995).

[33] G. S. Bales and D. C. Chrzan, Phys. Rev. Lett. **74**, 4879 (1995).

[34] T. R. Linderoth, J. J. Mortensen, K. W. Jacobsen, E. Laegsgaard, I. Stensgaard, and F. Besenbacher, Phys. Rev. Lett. **77** 87 (1996).

[35] O. Biham, M. Karimi, G. Vidali, R. Kennett, and H. Zeng (unpublished).

[36] M. C. Bartelt, S. Gunther, E. Kopatzki, R. J. Behm, and J. W. Evans, Phys. Rev. B **53**, 4099 (1996).

[37] M. C. Bartelt, L. S. Perkins, and J. W. Evans, Surf. Sci. Lett. **344**, L1193 (1995).

[38] G. L. Kellogg and A. F. Voter, Phys. Rev. Lett. **67**, 622 (1991); G. L. Kellogg, *ibid.* **73**, 1833 (1994).

[39] K. Falconer, *Fractal Geometry: Mathematical Foundations and Applications* (Wiley, Chichester, 1990).

[40] Z. Zhang, Y.-T. Lu, and H. Metiu, Surf. Sci. Lett. **255**, L543 (1991); K. Fichthorn and W. H. Weinberg, J. Chem. Phys. **95**, 1090 (1991).

[41] The diffusion coefficient for a monomer is given by Eq. (3) with $E_B = 0.5$ eV and $T = 250$ K. The result is $h_1 = 84$ hops/s. It can be shown that the dimer's diffusion coefficient $h_2$ satisfies $h_2 = h_1/4$.

[42] The scaling relation between $N$ and $F/h$ is in agreement with the result previously obtained in Ref. 17, where a different approach was used.

[43] D. A. Hamburger, A. T. Yinnon, and R. B. Gerber, Chem. Phys. Lett. **253**, 223 (1996); D. A. Hamburger-Lidar, Phys. Rev. E **54**, 354 (1996); A. T. Yinnon, D. A. Lidar (Hamburger), I. Farbman,

R. B. Gerber, P. Zeppenfeld, M. A. Krzyzowski and G. Comsa (unpublished).

[44] D. Kandel and E. Kaxiras, Phys. Rev. Lett. **75**, 2742 (1995).

[45] P. J. Feibelman, Phys. Rev. Lett. **65**, 729 (1990).

[46] G. L. Kellogg and P. J. Feibelman, Phys. Rev. Lett. **64**, 3143 (1990).

[47] Z.-P. Shi, Z. Zhang, A. K. Swan, and J. F. Wendelken, Phys. Rev. Lett. **76**, 4927 (1996).

[48] J.-M. Wen, S.-L. Chang, J. W. Burnett, J. W. Evans, and P. A. Thiel, Phys. Rev. Lett. **73**, 2591 (1994).

[49] P. Meakin, in *Phase Transitions and Critical Phenomena*, edited by C. Domb and J. L. Lebowitz (Academic, New York, 1988), Vol. 12, p. 344.

[50] T. Vicsek, *Fractal Growth Phenomena* (World Scientific, Singapore, 1989).

[51] P. Jensen, A.-L. Barabási, H. Larralde, S. Havlin, and H. E. Stanley, Phys. Rev. B **40**, 15 316 (1994).